Progress In Electromagnetics Research C, Vol. 118, 177–186, 2022

A Circular Sector with an Inverted L Shaped Monopole Antenna for Tri-Band Applications

Alka Khade, Mahadu Trimukhe, Shishir Jagtap, and Rajiv K. Gupta*

Abstract—In this paper, a quarter circular sector with an inverted L shaped monopole antenna for tri-band applications is proposed. The antenna is designed from a U shaped ultra-wideband (UWB) antenna. The number of higher-order modes, each with wide bandwidth, gets excited in a monopole, which electromagnetically couple to provide UWB. In the proposed tri-band antenna the electromagnetic coupling between higher-order modes is reduced by selectively removing the symmetrical portion and decreasing the thickness of the UWB radiator. An inverted L strip is added to a quarter circular sector, and a similarly shaped parasitic element is placed close to the radiator to achieve the desired tri-band. The antenna provides $S_{11} \leq -10$ dB over 2.1–2.5 GHz, 5.0–5.6 GHz and 8.4–9.0 GHz which covers 3G, Wi-Fi, LTE, Bluetooth, WLAN, and X-band applications. The antenna offers nearly omnidirectional radiation pattern in the lower band and directional radiation pattern in the other two bands. The prototype antenna is fabricated on a $0.147\lambda_0 \times 0.22\lambda_0$ FR4 substrate, where λ_0 is the free-space wavelength corresponding to 2.1 GHz. The measured results agree with simulation ones.

1. INTRODUCTION

In the modern era, rapid changes in wireless technologies need antennas that can support services such as Bluetooth, WLAN, UWB, and LTE, each operating over a different frequency band. Conventionally, multiple antennas operating over these bands are required. However, the usage of multiple antennas is restricted as it increases the size, volume, and cost. A wideband antenna covering all the bands is also not suitable as it covers unwanted frequency bands and causes interference. A multiband antenna in a mobile communication system operates at distinct frequency bands, with stopbands at the intermediate frequencies between passbands. Therefore, an antenna with multiband characteristics is desirable.

Multiband monopole antennas have been designed using multiple branches in which each branch resonates over a different band [1–6]. The effective length of a branch is about $\lambda/4$ where λ is the wavelength corresponding to resonating frequency of that branch. These branches are designed in different shapes like C-shape, L shape, U shape, or meander line shape to reduce the size of antenna. One or more branches are added to a branch to achieve multiple bands. Slot and slits are introduced in radiating element and ground plane to obtain the desired bandwidth [1–6]. A meander line branch is attached to a G shape monopole antenna to achieve tri-band operation [1]. A slot is cut in the ground plane to improve impedance matching over the desired bands. A quad-band monopole antenna is designed using four L shape branches [2]. A dual arc-shaped strip with dual inverted L-shaped parasitic stubs on the other side of the substrate is used to design a multiband antenna in [3]. A CPW-fed multi-branch antenna is proposed in [4]. A microstrip line fed tri-band pentagon-shaped monopole antenna with two symmetrical hooks and a slot is designed in [5], while a coaxial cable fed multi-band antenna is designed and accommodated above a laptop system ground in [6].

Received 8 January 2022, Accepted 8 February 2022, Scheduled 21 February 2022
* Corresponding author: Rajiv Kumar Gupta (rajivgupta@ternaengg.ac.in).
The authors are with the Department of Electronics and Telecommunication, Terna Engineering College, Navi-Mumbai, India.

Multiband antennas using split-ring resonator (SRR) and metamaterial have been reported [7–11]. A circularly polarized (CP) strip and SRR loaded tri-band slot antenna is reported in [7], while a multi-band CP annular ring antenna loaded with eight slots and octagonal closed ring resonators is designed in [8]. Resonant modes of SRR and strips are combined with the fundamental mode of the slot to produce circular polarization at the resonance frequencies. A meandered coplanar waveguide (CPW) fed complementary SRR (CSRR) loaded multiband antenna is proposed in [9]. A multiband hexagonal split-ring resonator (HSRR) enclosing a circular split-ring (CSR) is proposed for sub-6 GHz bands [10]. A metamaterial inspired antenna using CSRR is reported in [11]. CSRRs are employed to miniaturize the antenna.

Multiband antennas are also designed using fractal method [12–14]. By cutting a triangle slot in a circular monopole, a fractal circular nested triangle structure is presented for multiband operation in [12] whereas a dual-band binary branch fractal bionic antenna is reported in [13]. Multiband elliptical patch fractal with a defective ground plane is proposed in [14]. Frequency reconfigurable multi-band antennas have been reported [15–17]. A reconfigurable planar inverted F shape antenna (PIFA) with capacitive loaded slots is designed in [15]. Slots and strips are introduced in a monopole, and reconfigurability is achieved by using PIN diodes in order to enhance the device utility [16, 17].

In this paper, a novel single element multi-band antenna is designed from a UWB antenna on a low cost and easily available FR4 substrate. The antenna is designed by reducing the electromagnetic coupling between the higher-order modes by selectively cutting the symmetrical portion and reducing the thickness of the monopole. The antenna has neither multiple branches nor any complex SRR or meta-material, and thus, it is simple to design. The proposed single branch tri-band monopole antenna consists of a quarter circular sector and a rectangular inverted L strip. The antenna operates over 2.1–2.485 GHz band for Bluetooth (2.402–2.482 GHz), 3G, Wi-Fi (2.400–2.483 GHz), LTE 2300 (2.305–2.400 GHz) applications, 5.05–5.67 GHz band for WLAN application, and 8.4–9.0 GHz band for applications in X-band. The antenna resonates over the lower band in the fundamental mode, while it resonates over the middle and upper bands in the higher order modes. The antenna offers nearly omnidirectional radiation characteristics in the lower band and directional characteristics in the other two bands.

2. DESIGN THEORY AND ANTENNA GEOMETRY

A monopole antenna excites multiple higher-order modes, each with wide bandwidth, which electromagnetically couple to offer large impedance bandwidth [18]. The resonating frequency and bandwidth of the various modes depend on the shape of the radiator. The resonating frequencies of various modes of a circular monopole are closer to each other than a rectangular monopole. Therefore, electromagnetic coupling among the various modes of the circular monopole is more than the rectangular monopole. The bandwidth of a monopole also depends on the width of the monopole. Thus, the shape and width of a monopole are responsible for electromagnetic coupling between the modes. A multi-band monopole antenna can be designed by reducing the electromagnetic coupling between these modes, and the desired bands can be obtained by optimizing the geometry of the monopole antenna.

The geometry of the proposed antenna is shown in Fig. 1. The antenna consists of a quarter circular sector and a rectangular inverted L strip. A similarly shaped parasitic element is placed close to the radiator to provide capacitive effect and achieve the desired tri-band. A small portion of the circular arc to the right of the feed line improves the impedance matching. The parameters of the antenna are optimized. The detailed antenna dimensions are listed in Table 1. The antenna is designed on a 1.6 mm thick FR4 substrate. The dielectric constant and loss tangent of FR4 substrate are 4.4 and 0.02, respectively. The antenna is fed through a 50 Ω microstrip line. The structure is designed and simulated by using HFSS simulator. The prototype of the proposed antenna is fabricated to verify the simulated results. The top and bottom views of the fabricated antenna are shown in Fig. 2. The antenna occupies $32 \times 21\,\text{mm}^2$ board area and is realized using the printed circuit board etching technique.

The evolution stages of the proposed antenna and the simulated S-parameters of each stage are shown in Fig. 3 and Fig. 4, respectively. Initially, Antenna-1, a U-shaped monopole antenna, is designed on a 36 mm $\times$ 36 mm FR4 substrate to operate over UWB [19]. The structure is optimized. $S_{11} < -10$ dB is obtained from 2.6 GHz to 11.05 GHz. The antenna is symmetrical and consists of semi-circular and

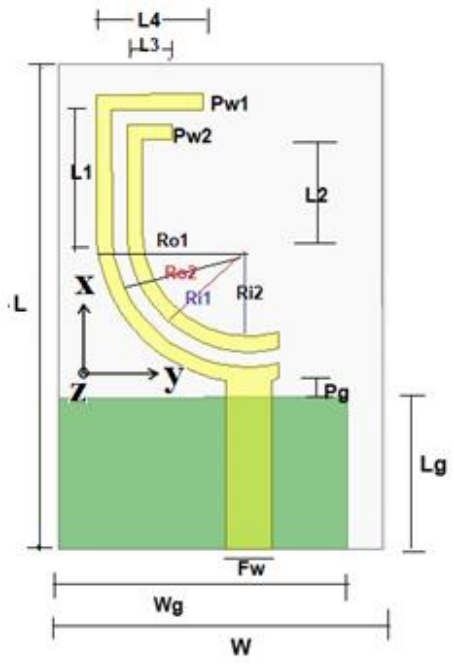

Figure 1. Geometry of the proposed antenna.

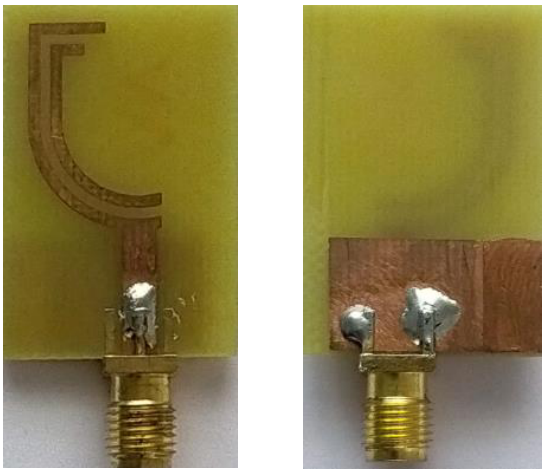

Figure 2. Fabricated prototype antenna.

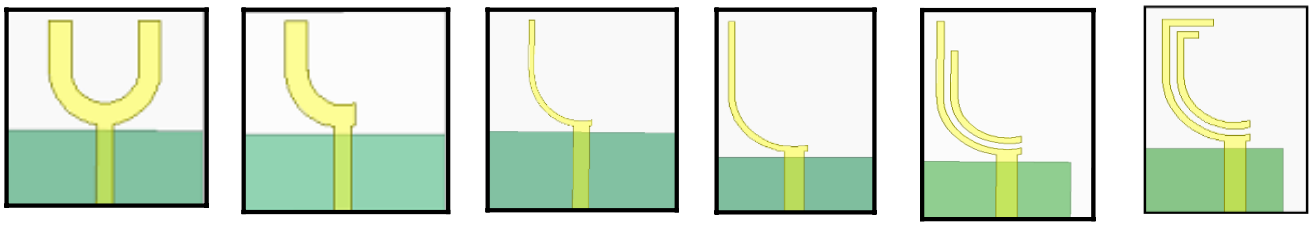

Figure 3. Evolution stages of the proposed antenna.

Table 1. Dimensions of the proposed antenna.

Parameter	L	W	L_g	W_g	P_g	Ro_1	Ro_2	Ri_1	Ri_2	L_1	L_2	L_3	L_4	Pw_1	Pw_2	F_w
Value (mm)	32	21	10	19	1	10	9	8	7	8	6	3	7	1	1	3

rectangular arms. The scalar surface current distributions of Antenna-1 at 3.3 GHz, 6.8 GHz, and 10.2 GHz are depicted in Fig. 5. The surface current is distributed symmetrically over UWB. The semi-circular arm of monopole antenna excites multiple higher-order modes, each with wide bandwidth, which electromagnetically couple to provide ultra-wide bandwidth. This coupling is reduced in Antenna-2 to achieve multiple bands.

In Antenna-2, slightly less than one half of the radiating element is removed. The structure still operates over multiple modes, but it offers triple bands. The small portion to the right of the feed line acts as a stub and improves the impedance matching. As the effective surface current density increases due to decrease in surface area in Antenna-2, the effective current path length increases; therefore, Antenna-2 resonates at lower frequency. Similar results are obtained when the left portion is removed instead of right portion of Antenna-1. In Antenna-3 the width of radiating arm is decreased from 4 mm

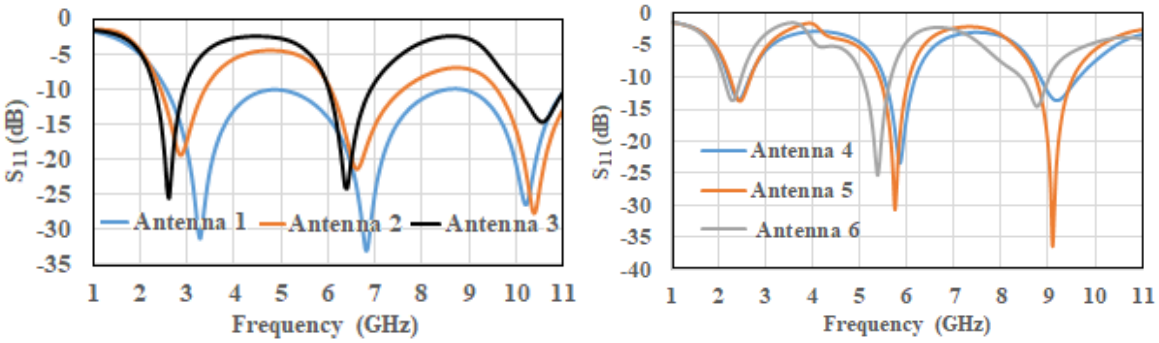

Figure 4. S_{11} of evolution stages of the proposed antenna.

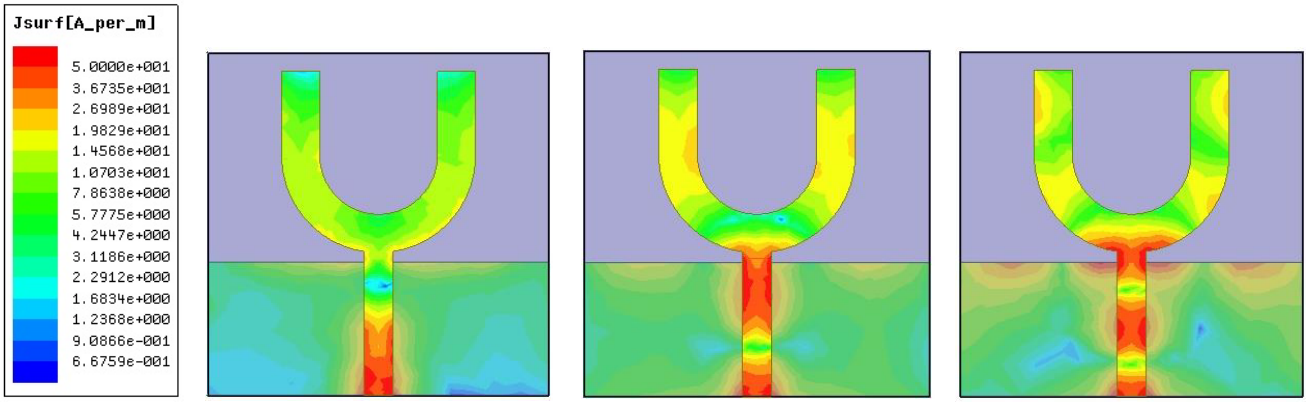

Figure 5. Surface current distribution (a) 3.3 GHz, (b) 6.8 GHz, (c) 10.2 GHz.

to 1 mm to further increase the surface current density and decrease the resonant frequency. Antenna-3 offers $S_{11} < -10$ dB over 2.32–2.95 GHz, 6.0–6.9 GHz, and 10.05–11.04 GHz.

In Antenna-4 the length of the rectangular radiating arm is increased. As a result, the resonant frequencies of middle and upper bands decrease which indicates that the circular sector arm controls the lower band while the rectangular arm affects the middle and upper bands. However, increase in the length of rectangular arm increases the dimensions of the antenna.

In Antenna-5 a parasitic arm similar to radiating arm is placed at a distance of 1 mm from the radiating arm. The parasitic arm electromagnetically couples with the radiating arm. However, the radiating and parasitic arms couple tightly over the lower band due to less electrical spacing. As a result, there is a negligible effect on the resonant frequency of lower band, but resonant frequency of middle and upper bands decreases due to capacitance between the parasitic and radiating arms. Besides adding a parasitic arm, the ground plane is cut from the right to reduce the size of the antenna.

In the proposed antenna, Antenna-6, the rectangular radiating and parasitic arms are bent to further reduce the size of antenna. The structure is optimized so that it operates over the desired bands from 2.1–2.5 GHz, 5.0–5.6 GHz, and 8.4–9.0 GHz. The resonant frequency and bandwidth of three bands depend on the number of parameters, viz. ground plane length and width, the gap between radiating patch and ground plane, the radius and thickness of circular sector and parasitic element, the spacing between the radiating and parasitic elements, and the length and width of inverted L arm of radiating and parasitic elements. Parametric study is carried out to analyze the effect of different parameters.

In monopole antenna, the ground plane dimensions affect the resonating frequency and impedance bandwidth. The resonant frequencies of three bands increase slightly with increase or decrease in

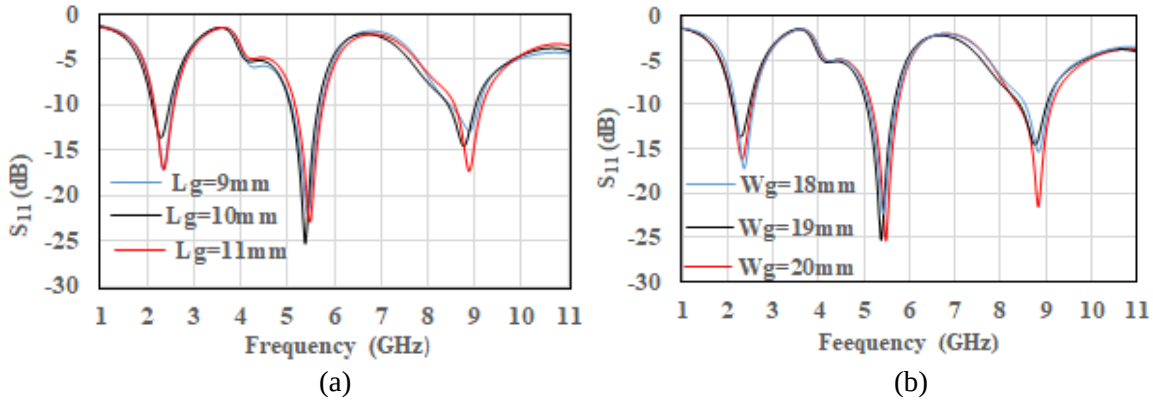

Figure 6. S_{11} (a) different ground plane length, (b) different ground plane width.

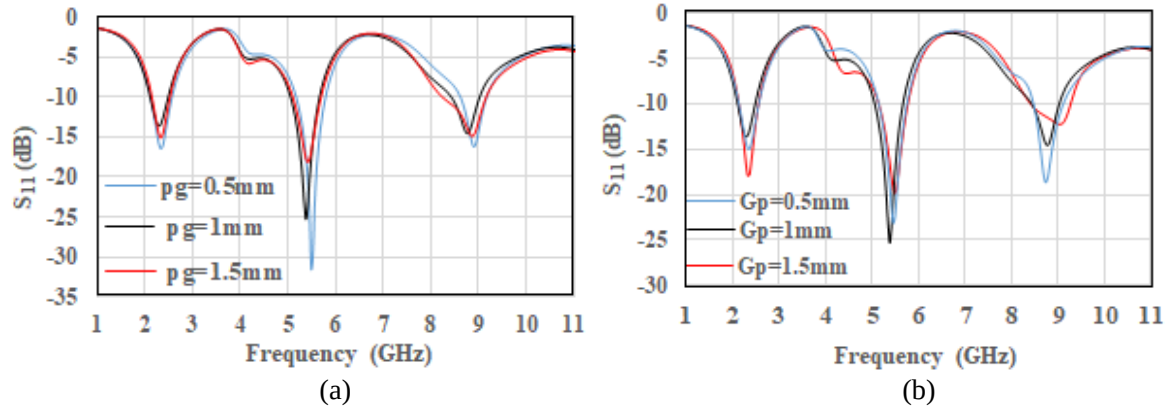

Figure 7. S_{11} (a) different P_g, (b) different G_p.

ground plane length 'L_g' and width 'W_g'. S_{11} for different 'L_g' and 'W_g' are shown in Fig. 6. The gap between the radiating patch and ground plane 'P_g' acts as a matching network. The spacing between the radiating patch and the ground plane is equivalent to a capacitor, and the metallic strip acts as an inductor. The gap between the radiating element and the ground plane also depends on the radiating element. S_{11} for different 'P_g' is shown in Fig. 7.

The gap 'G_p' between the radiating and parasitic elements has little effect on the lower band; however, it affects the middle and upper bands. As the electrical spacing is less at lower band, the two elements couple tightly and thus affect the bandwidth and resonant frequency marginally. However, as the electrical spacing increases with frequency, it affects the middle and upper bands. The structure acts as a single strip and provides omnidirectional radiation pattern at lower band but provides directional radiation pattern in middle and upper bands as the parasitic element acts as a director. The gap between two elements controls the middle and upper bands without affecting the lower band. S_{11} for different 'G_p' is shown in Fig. 7.

The impedance bandwidth of three bands increases with decrease in the width of radiating element '$Pw1$'. As the effective surface current density increases with decrease in the width of outer ring, the effective current path length increases; therefore, the resonant frequency of three bands also decreases with decrease in the width of outer ring as shown in Fig. 8.

The impedance bandwidth of lower and upper bands increases with increase in the width of parasitic element '$Pw2$'. The resonant frequency of three bands also increases with an increase in the width of the inner ring due to decrease in surface current density and effective current path length as shown in Fig. 8. However, the effect of width of inner ring is comparatively more in middle and upper bands than in lower band.

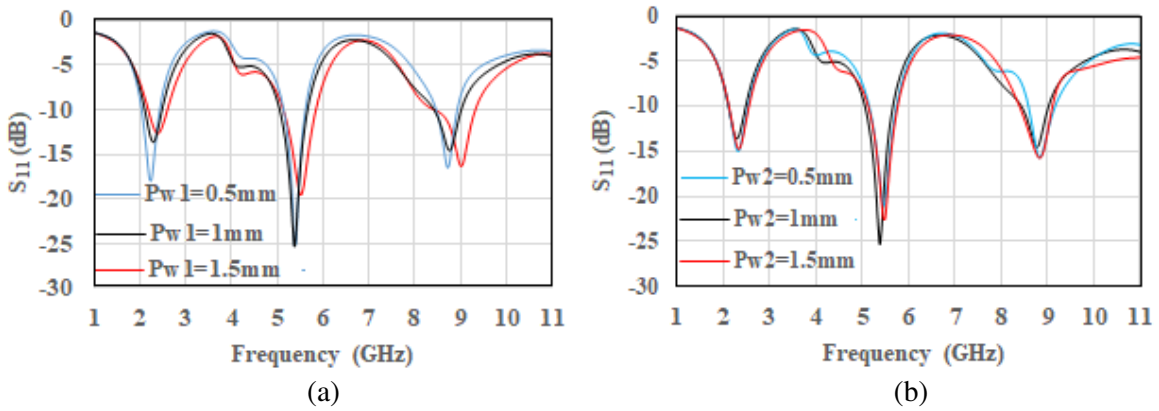

Figure 8. S_{11} (a) different $Pw1$, (b) different $Pw2$.

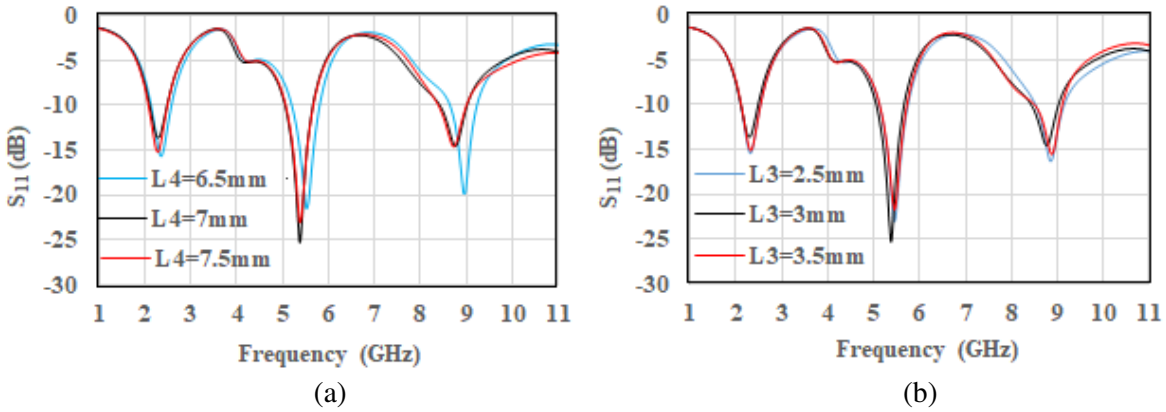

Figure 9. S_{11} (a) different $L4$, (b) different $L3$.

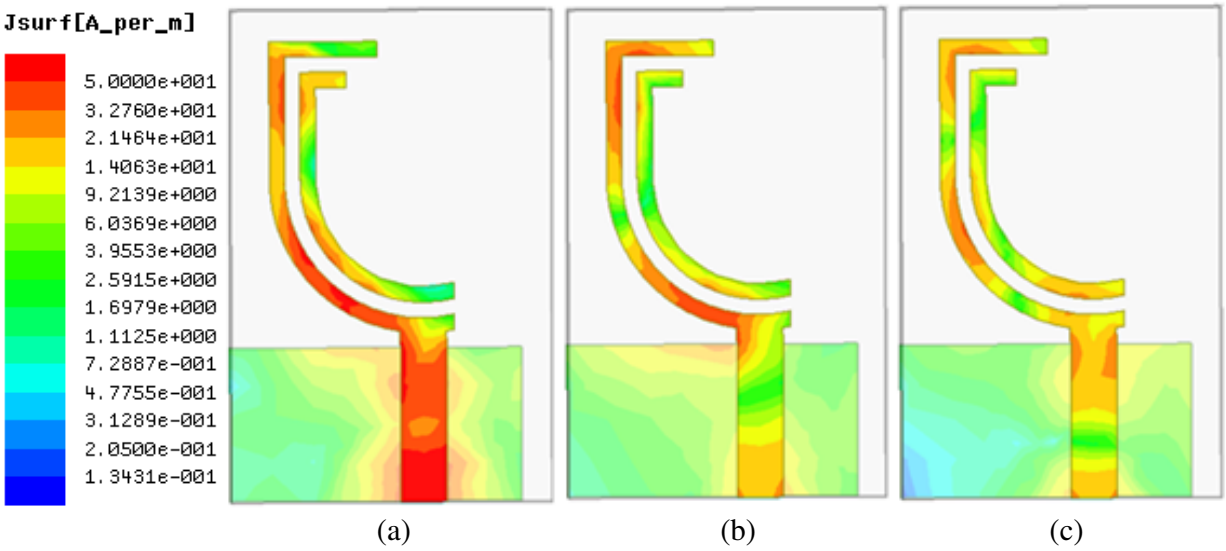

Figure 10. Surface current distribution (a) 2.3 GHz, (b) 5.4 GHz, (c) 8.8 GHz.

The effect of length of horizontal strip of radiating '$L4$' and parasitic '$L3$' is analyzed. The resonant frequency of three bands decreases with increase in '$L4$' due to increase in the effective current path length. Since the inner strip is parasitic, its effect on resonant frequency is marginal, for small variation in the length of inner strip '$L3$' at lower band; however, it affects the middle and upper bands as shown

in Fig. 9.

The tri-band operation and radiation mechanism of antenna can be explained with the help of surface current distribution. The scalar surface current distributions of the proposed antenna at 2.3 GHz, 5.4 GHz, and 8.8 GHz are depicted in Fig. 10. In the lower band, the entire radiating arm resonates in the fundamental mode. The parasitic arm is tightly coupled to the radiating arm. The surface current is distributed over the circular sector and the inverted L strip. Therefore, the lowest frequency f_L

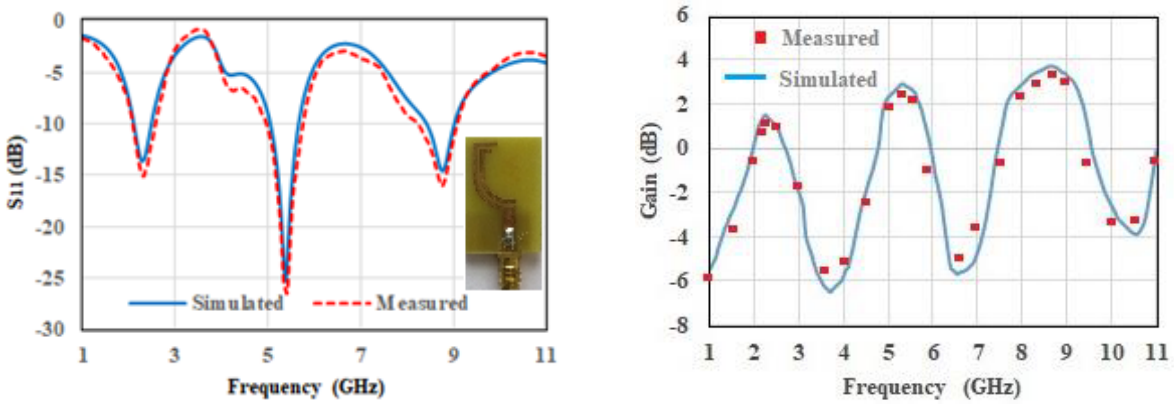

Figure 11. Measured and simulated (a) S_{11}, (b) gain.

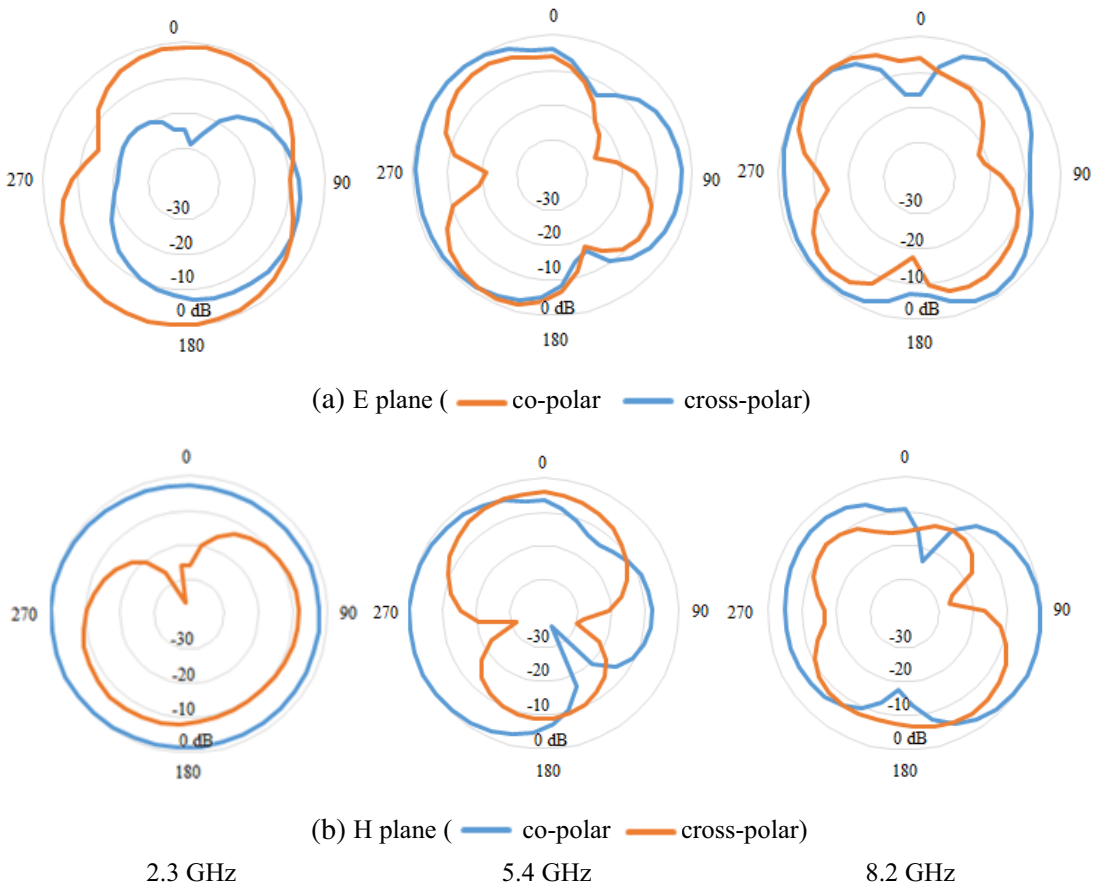

Figure 12. Radiation patterns of proposed antenna.

(corresponding to $S_{11} = -9.5\,\text{dB}$) can be given by

$$f_L = 7.2/\left(P_g + 0.25\pi\left(R_{01} + R_{02}\right) + L1 + L4\right) \times k \quad (1)$$

Here, f_L is in GHz, and dimensions of all parameters are in centimeter. The value of $k = 1.15$ is considered for the FR-4 substrate [20]. The calculated value of the lowest frequency f_L using Eq. (1) is

Table 2. Comparison of proposed antenna with state of art reported multiband antennas.

Ref	Approach/Technique	Antenna Size (mm^2)	Bands (GHz)	Electrical Size ($\lambda_o \times \lambda_o$)
[1]	Triple-branch antenna for tri-band operation, defected ground to improve impedance bandwidth	23×20	2.39–2.52 3.3–4.47 5.15–6.0	$0.18 \times 0.15 = 0.027\lambda_o^2$
[2]	Quad branch antenna for quad-band operation, asymmetrical feed	50×35.5	1.43–1.60 1.94–2.10 2.40–2.57 3.45–3.6	$0.24 \times 0.33 = 0.0792\lambda_o^2$
[3]	Two arc shaped branches with dual inverted stub for dual band operation	18×34.5	2.28–2.57 5.0–6.27 7.11–7.96	$0.1368 \times 0.262 = 0.0359\lambda_o^2$
[4]	Triple branch radiator for tri-band operation, asymmetrical ground plane	17×23.5	2.4/5.2/5.8	$0.136 \times 0.188 = 0.0256\lambda_o^2$
[5]	Pentagon shaped monopole with vertical slot and two hooked branches for tri-band operation	18×35	3.2–4.1 5.1–5.9 7.3–8.9	$0.192 \times 0.374 = 0.0717\lambda_o^2$
[7]	slot antenna loaded with metallic strips and a SRR	50×50	1.48–1.87 2.39–2.71 3.02–3.16	$0.247 \times 0.247 = 0.061\lambda_o^2$
[8]	Slots and CRR	35×30	4.08–5.05 5.98–13.6	$0.476 \times 0.408 = 0.1942\lambda_o^2$
[9]	Meandered CPW fed CSRR loaded	26×23	4.23–4.32 5.15–6.12 7.06–7.29	$0.367 \times 0.3243 = 0.119\lambda_o^2$
[10]	Hexagonal Split-Ring Resonator Circular Split-Ring Resonator	20×27	3.225–3.850 4.820–6.850	$0.215 \times 0.290 = 0.0624\lambda_o^2$
[11]	rectangle-shaped complementary split ring radiating element with an offset fed microstrip line	19×19	2.98–3.02 3.58–3.62 4.93–6.4	$0.189 \times 0.189 = 0.036\lambda_o^2$
[12]	circular antenna with triangular fractals	87.5×61	1.8–2.9 3.4–4.6 5–5.6	$0.525 \times 0.366 = 0.192\lambda_o^2$
[13]	binary tree fractal bionic structure	50×40	1.85–2.9 4.9–5.5	$0.308 \times 0.247 = 0.076\lambda_o^2$
[14]	Fractal antenna with defected ground structure	50×50	2.3–2.74 5.46–6.53 7.60–12.44	$0.384 \times 0.384 = 0.1472\lambda_o^2$
PA	Single branch antenna for tri-band operation, parasitic element	32×21	2.1–2.485 5.05–5.67 8.4–9.0	$0.224 \times 0.147 = 0.0329\lambda_o^2$

2.06 GHz which is close to the simulated frequency of 2.1 GHz.

Surface current distributions at 5.4 GHz and 8.8 GHz show that the antenna resonates in higher-order modes. The decrease in surface current in the parasitic arm at 5.4 GHz and 8.8 GHz depicts that the coupling between the two arms decreases with frequency.

3. FABRICATION AND MEASURED RESULTS

The fabricated prototype is shown in Fig. 2. The return loss (S_{11}) is measured using 9916A Agilent network Analyzer. Simulated and measured S_{11} parameters are shown in Fig. 11(a), while measured and simulated gains of the antenna are shown in Fig. 11(b). The gain variation over each operating band is less than 1 dB. The measured results are in agreement with simulated ones. The measured radiation patterns in E-plane (X-Z plane) and H-plane (Y-Z plane) at 2.3 GHz, 5.4 GHz, and 8.3 GHz are shown in Fig. 12. The radiation pattern is nearly omnidirectional in the H-plane and figure of eight in the E plane at 2.3 GHz. The radiation pattern becomes directive at 5.4 GHz as parasitic elements act as director at 5.4 GHz. The radiation pattern degrades at higher frequencies due to the excitation of higher-order modes. The cross-polar component increases with frequency due to increase in electrical thickness of the substrate and surface waves [21].

4. COMPARISON WITH STATE OF ART ANTENNAS

The proposed antenna (PA) is compared with state of art antennas reported in the literature with respect to size and the techniques used for designing multiband antenna in Table 2. The substrate dimensions of the proposed antenna are smaller than all the reported antennas except [1, 4]. The antennas in [1–4] are designed using multiple branches for multiband operation while the proposed tri-band antenna is designed using a single branch. The antenna in [5] is designed using a pentagon patch with slots and hook branches, and thus it is more complex to design and larger in size than the proposed antenna. The antennas in [6–11] are designed using SRR or CSRR while antennas in [12–14] are designed using fractal techniques. All these antennas [6–14] not only are difficult to design but also have larger dimensions. The proposed single branch antenna is designed by reducing the electromagnetic coupling between the higher-order modes by selectively cutting the symmetrical portion and reducing the thickness of the monopole. The antenna has neither multiple branches nor any complex SRR or meta-material, and thus, it is simple to design.

5. CONCLUSION

A novel single branch triband antenna is designed by reducing the electromagnetic coupling between the higher-order modes by selectively cutting the symmetrical portion and reducing the thickness of a U shaped UWB monopole. The proposed antenna operates over 2.1–2.485 GHz, 5.05–5.67 GHz, and 8.4–9.0 GHz bands. The antenna resonates over the lower band in the fundamental mode, while it resonates over the middle and upper bands in the higher order modes. The low-cost antenna is simple to design. The antenna offers nearly omnidirectional radiation characteristics in the lower band and directional characteristics in the other two bands. The gain variation over each operating band is less than 1 dB. Thus, the proposed antenna is suitable for Bluetooth, 3G, Wi-Fi, LTE 2300, WLAN, and X-band applications.

REFERENCES

1. Zaman, W., H. Ahmad, and H. A Mahmood, "Miniaturized meandered printed monopole antenna for triband applications," *Microwave and Optical Technology Letters*, Vol. 60, No. 5, 1265–1271, 2018.
2. Brar, R. S., K. Saurav, D. Sarkar, and K. V. Srivastava, "A quad-band dual-polarized monopole antenna for GNSS/UMTS/WLAN/WiMAX applications," *Microwave and Optical Technology Letters*, Vol. 60, No. 3, 538–545, 2018.

3. Zhi, R., M. Han, J. Bai, W. Wu, and G. Liu, "Miniature multiband antenna for WLAN and X-band satellite," *Progress In Electromagnetics Research Letters*, Vol. 75, 13–18, 2018.
4. Osklang, P., C. Phongcharoenpanich, and P. Akkaraekthalin, "Triband compact printed antenna for 2.4/3.5/5 GHz WLAN/WiMAX applications," *International Journal of Antennas and Propagation*, Article ID 8094908, 2019.
5. Mallat, N. K. and A. Iqbal, "Multi-band printed antenna for portable wireless communication applications," *Progress In Electromagnetics Research Letters*, Vol. 84, 39–46, 2019.
6. Kulkarni, J., "Multi-band printed monopole antenna conforming bandwidth requirement of GSM/WLAN/WiMAX standards," *Progress In Electromagnetics Research Letters*, Vol. 91, 59–66, 2020.
7. Paul, P. M., K. Kandasamy, and M. S. Sharawi, "A tri-band circularly polarized strip and SRR loaded slot antenna," *IEEE Transactions on Antennas and Propagation*, Vol. 66, No. 10, 5569–5573, 2018.
8. Dhara, R. and M. Monojit, "A triple-band circularly polarized annular ring antenna with asymmetric ground plane for wireless applications," *Engineering Reports*, Vol. 2, No. 4, e12150, 2020, doi: 10.1002/eng2.12150.
9. Pandeeswari, R., "Complimentary split ring resonator inspired meandered CPW-fed monopole antenna for multiband operation," *Progress In Electromagnetics Research C*, Vol. 80, 13–20, 2018.
10. Rajalakshmi, P. and N. Gunavathi, "Hexagonal split ring resonator enclosed circular split ring resonator inspired dual-band antenna for sub-6 GHz 5G NR and IEEE 802.11ba/be applications," *Progress In Electromagnetics Research C*, Vol. 115, 1–15, 2021.
11. Murugeshwari, B., R. S. Daniel, and S. Raghavan, "Metamaterial inspired structure with offset-fed microstrip line for multi band operations," *Progress In Electromagnetics Research M*, Vol. 82, 95–105, 2019.
12. Wang, L., J. Yu, T. Xie, and K. Bi, "A novel multiband fractal antenna for wireless application," *International Journal of Antennas and Propagation*, Article ID 9926753, 2021.
13. Ran, X., Z. Yu, T. Xie, Y. Li, X. Wang, and P. Huang, "A novel dual-band binary branch fractal bionic antenna for mobile terminals," *International Journal of Antennas and Propagation*, Article ID 6109093, 2020.
14. Kaur, A. and P. K. Malik, "Multiband elliptical patch fractal and defected ground structures microstrip patch antenna for wireless applications," *Progress In Electromagnetics Research B*, Vol. 91, 157–173, 2021.
15. Asadallah, F. A., J. Costantine, and Y. Tawk, "A multiband compact reconfigurable PIFA based on nested slots," *IEEE Antennas and Wireless Propagation Letters*, Vol. 17, 331–334, 2018.
16. Singh, P. P., P. K. Goswami, S. K. Sharma, and G. Goswami, "Frequency reconfigurable multiband antenna for IoT applications in WLAN, Wi-MAX, and C-band," *Progress In Electromagnetics Research C*, Vol. 102, 149–162, 2020.
17. Bharadwaj, S. S., D. Sipal, D. Yadav, and S. K. Koul, "A compact tri-band frequency reconfigurable antenna for LTE/Wi-Fi/ITS applications," *Progress In Electromagnetics Research M*, Vol. 91, 59–67, 2020.
18. Kumar, G. and K. P. Ray, *Broadband Microstrip Antennas*, Artech House, Norwood, MA, 2003.
19. Mishra, S. K., R. K. Gupta, A. Vaidya, and J. Mukherjee, "A compact dual-band fork-shaped monopole antenna for Bluetooth and UWB applications," *IEEE Antennas Wireless Propagation Letters*, Vol. 10, 627–630, 2011.
20. Ray, K. P., "Design aspects of printed monopole antennas for ultra-wide band applications," *International Journal of Antennas and Propagation*, Vol. 2008, 1–8, 2008.
21. Mishra, S. K., R. K. Gupta, and J. Mukherjee, "Effect of substrate material on radiation characteristics of an UWB antenna," *Loughborough Antennas & Propagation Conference*, 157–160, U.K., 2010.